ADVANCED FUNCTIONAL MATERIALS
www.afm-journal.de



# mRNA-Loaded Lipid-Like Nanoparticles for Liver Base Editing Via the Optimization of Central Composite Design

*Qian Zheng, Fengming Qin, Ruijie Luo, Chaohui Jin, Hai Huang, He Xi, Wen Xiao, Mengran Guo, Shuping Yang, Siyan He, Lizhi Cheng, Na Fan, Shaohua Yao,* and Xiangrong Song**

**Messenger RNA (mRNA) has come into the spotlight due to its potential for addressing a staggering number of diseases, while the lack of effective and safe carriers for in vivo delivery significantly limits its clinical application. Herein, the potential of lipid-like nanoparticles (LLNs) containing three new cholesterol derivatives to achieve the liver targeting delivery of mRNA is investigated. The central composite design (CCD) is used to tailor the formulation of LLNs through in vivo optimization of the molar ratios of these cholesterol derivatives required for liver targeting. The optimized LLNs (O-LLNs) are able to systemically deliver mRNA to the liver of mice with a synergistic action of prolonged systemic circulation, increased liver targeting, and enhanced hepatocyte uptake. The O-LLNs outperformed DLin-MC3-DMA (MC3) in functional delivery of Cre-recombinase (Cre) and human erythropoietin (hEPO) mRNA. Successful delivery of cytidine base editor mRNA (CBE mRNA) and sgRNA by O-LLNs achieved more than 8% correction rates in a liver-related metabolism disorder, phenylketonuria (PKU). In conclusion, the general method above can accelerate in vivo screening and optimization of multicomponent nanoparticle formulations, and the optimized ones demonstrate great potential as delivery vehicles for targeted gene therapy in specific tissues.**

## 1. Introduction

In vivo delivery of messenger RNA (mRNA) has been widely explored for gene replacement[1–3] and clustered regularly interspaced short palindromic repeats-CRISPR-associated proteins (CRISPR-Cas)-based gene editing for genetic diseases.[4–6] Established on the traditional CRISPR-Cas systems, the newly-developed base editor systems can realize precise single nucleotide conversion independent of a double-strand DNA break and homology-directed repair (HDR) donors.[7,8] However, the current delivery of base editor generally resorts to viral vectors.[9,10] Despite promising delivery efficiency, the use of viral systems can be limited by cost, restricted packing capacity, and safety issues.[11–13] In comparison, non-viral nanocarriers provide safe and versatile platforms for transient mRNA delivery.[2] Recently, nonviral delivery systems including lipid nanoparticles (LNPs)[14,15] and lipid-like nanoparticles (LLNs)[16] have been explored for in vivo base editing, but a large body of works on the optimization of non-viral carriers are required to improve efficient and specific targeting base editing of mRNA in vivo.

To date, a few recent researches tried to optimize carrier formulations for efficient mRNA delivery to specific tissues.[17] For example, orthogonal experimental design (OED) was utilized to identify the optimal LLNs or LNPs formulations with the greatest transfection efficiency in vitro. These optimal formulations finally showed enhanced mRNA expression efficiency in liver after systemic delivery in mice.[18–20] Anderson and co-workers successfully deliver mRNA to liver,[21] lymph nodes,[22] and lungs[23] with the fractional factorial and definitive screening designs. In addition, library screening approaches were also used to determine the basic key structure, followed by optimizing the structure for tissue-specific mRNA delivery,[24–26] which might be time-consuming and laborious. Recently, a high-throughput method was taken to accelerate the discovery of clinically relevant mRNA delivery platforms from libraries of nanoparticles.[27–29] Central composite design (CCD) is a multi-factor five-level experimental design, which is formed by adding extreme points and center points on the basis of a two-level factorial design. Compared with experimental designs above, CCD shows an advantage of optimizing multicomponents with an optimum number of experimental runs by establishing quadratic models.[30] Therefore, we aimed to develop LLNs containing simple cholesterol derivatives for liver-targeted mRNA delivery via in vivo optimization based on CCD.

The optimized LLNs (O-LLNs) by CCD succeeded in functional delivery of Cre-recombinase (Cre) mRNA, human erythropoietin (hEPO), and mCherry mRNA, respectively.

Q. Zheng, F. Qin, R. Luo, C. Jin, H. Huang, H. Xi, W. Xiao, M. Guo, S. Yang, S. He, L. Cheng, N. Fan, Prof. S. Yao, Prof. X. Song
Department of Critical Care Medicine
Frontiers Science Center for Disease-related Molecular Network
State Key Laboratory of Biotherapy and Cancer Center
West China Hospital
Sichuan University
No.17, Section 3, Renmin South Road, Chengdu, China
E-mail: shaohuayao@scu.edu.cn; songxr@scu.edu.cn

The ORCID identification number(s) for the author(s) of this article can be found under https://doi.org/10.1002/adfm.202011068.

**DOI: 10.1002/adfm.202011068**

Subsequently, the base editing efficacy mediated by cytidine base editor mRNA-loaded O-LLNs reached >8% in human phenylketonuria (PKU) model mice (*Pah*$^{enu2}$). Together, this study might provide a potential and universal design platform for the development of non-viral gene carriers with efficient and specific targeting delivery, especially based on simple biomaterials with facile production and good prospect of clinical translation.

## 2. Results and Discussion

### 2.1. Functional Verification of Three Cholesterol Derivatives

The mRNA delivery systems for systemic administration often require multifunctions including macrophage phagocytosis evasion, accumulation in targeted tissues, and endocytosis by targeted cells.[31] To achieve such stage-by-stage delivery, we designed three functional cholesterol conjugates termed Chol-PEG$_{400}$-selfpeptide (Chol-PEG$_{400}$-SP), Chol-PEG$_{400}$-Mannose (Chol-PEG$_{400}$-Man), and Chol-PEG$_{2000}$-W$_5$R$_4$K (Chol-PEG$_{2000}$-WRK), respectively (**Figure 1**A). These structures were confirmed by $^1$H NMR (Figures S1–S3, Supporting Information). The ionizable lipid G0-C14 was prepared for mRNA complexation in light of the literature.[32] mRNA can be encapsulated into LLNs via electrostatic attraction with the cationic head groups of G0-C14. The obtained conjugates with different molar ratios were incorporated into LLNs by a thin film-dispersion method and mRNA was finally encapsulated in the LLNs via electrostatic attraction (Figure 1B). When LLNs systemically distribute into the bloodstream, Chol-PEG$_{400}$-SP on the surface provided a "don't eat me" signal to macrophages through signal regulatory protein (SIRP) $\alpha$ to prevent non-specific phagocytosis. Chol-PEG$_{400}$-Man subsequently enhanced mRNA accumulation in liver through ligand-receptor interactions mediated by mannose receptors (MR) on liver sinusoidal endothelial cells (LSECs). Finally, Chol-PEG$_{2000}$-WRK may facilitate LLNs uptake into hepatocytes.

We first verified the effects of the Chol-PEG$_{400}$-SP, Chol-PEG$_{400}$-Man, and Chol-PEG$_{2000}$-WRK on LLNs-mediated mRNA delivery, respectively. CD47 is a glycoprotein expressed on cell surface. Its extracellular domain could interact with SIRP$\alpha$ receptor in macrophages, leading to tyrosine phosphorylation of the immunoreceptor tyrosine-based inhibitory motifs and a subsequent inhibition of phagocytosis.[33–35] The ectodomain of CD47 and specific peptides derived from the SIRP$\alpha$-binding region of CD47 were able to reduce phagocytosis and clearance of carriers both in vitro and in vivo.[33,36] The selfpeptide (SP, GNYTCEVTELTREGETIIELK) is a minimal SIRP$\alpha$ binding-site derived from CD47. SP-modified nanoparticles were reported to be capable of delaying macrophage-mediated clearance and promote persistent circulation after i.v. injection.[37] SP-conjugated cholesterol (Chol-PEG$_{400}$-SP) was designed for the first time to construct functional luciferase (Luc) mRNA-loaded LLNs (S-LLNs/Luc and SMW-LLNs/Luc). The effect of Chol-PEG$_{400}$-SP on LLNs' uptake by macrophages was quantified using Cy5-labelled mRNA (Cy5 mRNA) in vitro. The macrophage-like Raw264.7 cells were incubated with 0.5 μg Cy5 mRNA-loaded LLNs for 2 h. Detected by confocal laser scanning microscope (CLSM) and flow cytometry (FACS), SMW-LLNs/Cy5, containing Chol-PEG$_{400}$-SP, Chol-PEG$_{400}$-Man, and Chol-PEG$_{2000}$-WRK, showed lower internalization efficiency compared with MW-LLNs/Cy5 without Chol-PEG$_{400}$-SP (**Figure 2**A and Figure S4, Supporting Information), implying that Chol-PEG$_{400}$-SP inhibited phagocytosis of Raw264.7 cells. This hypothesis was further verified by a competitive inhibition in which free SP was able to increase the internalization of Chol-PEG$_{400}$-SP-containing LLNs/Cy5 but had no influence on Chol-PEG$_{400}$-SP-free LLNs/Cy5 (Figure S5, Supporting Information).

We also tried to enhance the delivery of LLNs in liver based on the over-expressing mannose receptors on LSECs. Mannose receptors have been confirmed to abundantly present on LSECs and dendritic cells.[38–40] The carbohydrate recognition region of the mannose receptor can specifically recognize and bind carbohydrate compounds containing mannose, *N*-acetylglucosamine, and trehalose.[41–43] In this study, mannose-modified cholesterol (Chol-PEG$_{400}$-Man) was designed for the first time to construct liver-targeting LLNs (M-LLNs/Luc and SMW-LLNs/Luc). The biodistribution of DiD-labelled LLNs was investigated to verify the effect of this cholesterol derivative in vivo. The ex vivo fluorescence images showed that Chol-PEG$_{400}$-Man led to more accumulation in the liver 2 h post-intravenous injection, which was consistent with previous studies.[44] The fluorescence intensity of SMW-LLNs/DiD in the liver was higher than that of the SW-LLNs/DiD group (without Chol-PEG$_{400}$-Man) (Figure 2B). These results indicated that the mannose modification greatly improved liver targeting efficacy of the LLNs. Additionally, the dendritic cell line DC2.4 overexpressing mannose receptors was employed to mimic LSECs in order to explore the binding characteristics of Chol-PEG$_{400}$-Man and mannose receptors. As shown in Figure S6, Supporting Information, Chol-PEG$_{400}$-Man containing LLNs/Cy5 presented significantly higher intracellular uptake than Chol-PEG$_{400}$-Man-free LLNs/Cy5 according to the quantified mean fluorescence intensity of Cy5. The uptake of O-LLNs/Cy5 dramatically decreased in the presence of an excess of mannose at 37 °C. However, the introduction of mannose caused no significant change in the uptake of Chol-PEG$_{400}$-Man-free LLNs/Cy5. These results suggested that Chol-PEG$_{400}$-Man in LLNs had a high affinity for mannose receptor and played an essential role in LSECs-mediated liver accumulation.

WRK is an amphipathic homochiral L-cyclic peptide containing 5 tryptophan, 4 arginine, and 1 lysine residues. As one of cyclic cell penetrating peptides, WRK has the potential to achieve better enzymatic stability and enhances the cellular uptake more efficiently in contrast to linear cell penetrating peptides such as transactivator, penetratin, and arginine-rich peptides,[45–47] Hence, we synthesized Chol-PEG$_{2000}$-WRK for the first time to construct uptake-enhancing LLNs (W-LLNs/Luc and SMW-LLNs/Luc). We explored the effect of WRK-conjugated cholesterol (Chol-PEG$_{2000}$-WRK) on the cellular internalization of mRNA-loaded LLNs. The in vitro cell uptake study of Cy5 mRNA-loaded LLNs was performed in human hepatocytes (LO2 cells). SMW-LLNs/Cy5 exhibited higher uptake by LO2 cells compared with SM-LLNs/Cy5 (without Chol-PEG$_{2000}$-WRK) (Figure 2C and Figure S7, Supporting Information), demonstrating that the cyclic peptide WRK efficiently enhanced the uptake of mRNA by hepatocytes.

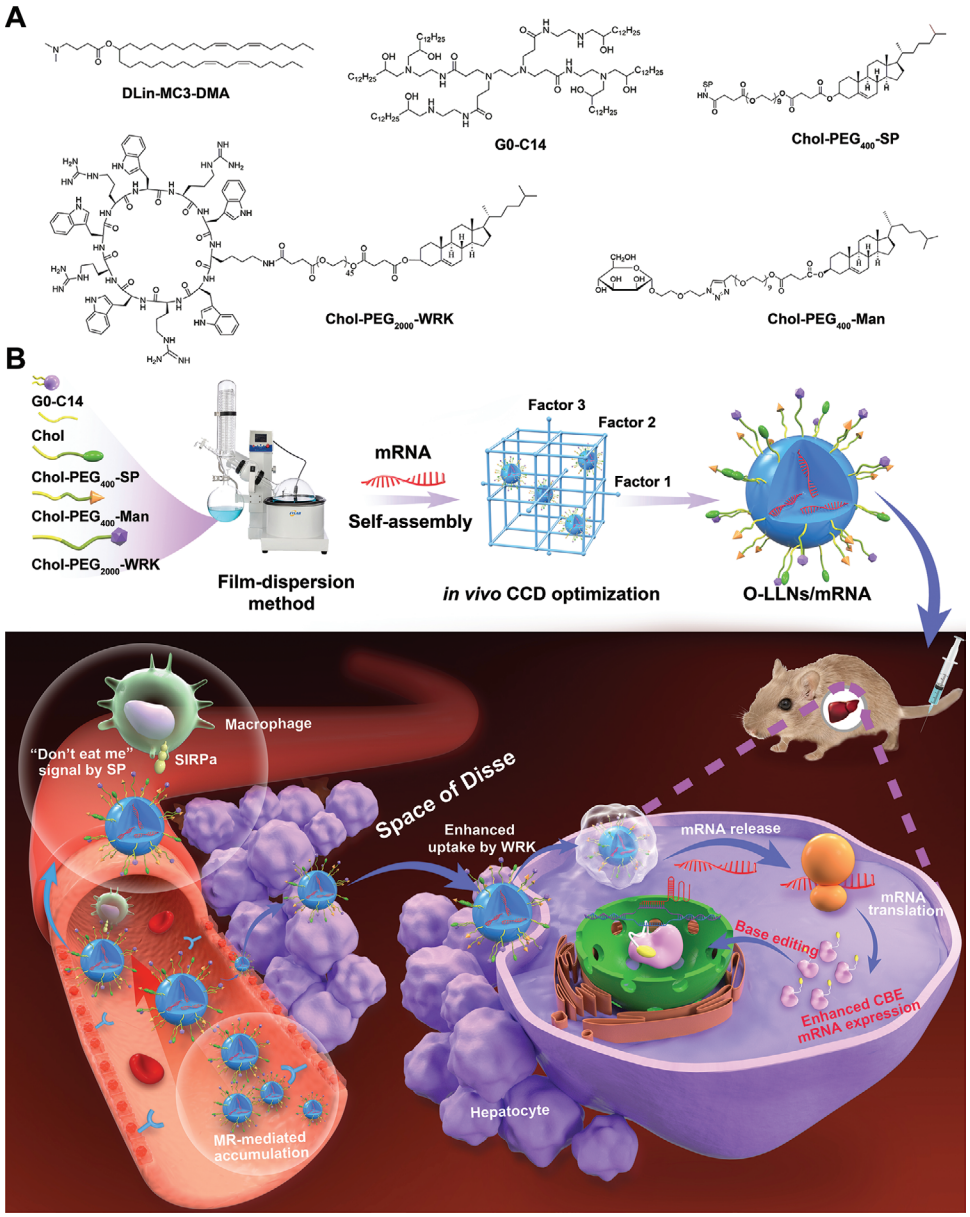


**Figure 1.** Schematic illustration of preparation, optimization and liver-targeted delivery of mRNA-loaded LLNs. A) Chemical structures of DLin-MC3-DMA (MC3), G0-C14, Chol-PEG$_{400}$-SP, Chol-PEG$_{2000}$-WRK, and Chol-PEG$_{400}$-Man. B) LLNs were prepared by a thin film-dispersion method and negatively charged mRNA was encapsulated in positively charged LLNs through self-assembly. CCD was applied to obtain O-LLNs for liver-targeted mRNA delivery in vivo. After the systemic administration of O-LLNs/mRNA, Chol-PEG$_{400}$-SP on the surface of O-LLNs provided a "don't eat me" signal to macrophages through SIRP$\alpha$ to prevent non-specific phagocytosis. Subsequently, Chol-PEG$_{400}$-Man interacted with mannose receptors (MR) expressing on LSECs, thereby enhancing O-LLNs accumulation in the liver. Finally, Chol-PEG$_{2000}$-WRK facilitated LLNs uptake into hepatocytes, thus leading to enhanced protein expression and base editing. Factor 1: Chol-PEG$_{400}$-SP, factor 2: Chol-PEG$_{400}$-Man, factor 3: Chol-PEG$_{2000}$-WRK.

Finally, we performed a distribution test to investigate the effect of three functional derivatives on mRNA expression. Distribution of Luc mRNA was evaluated in Balb/c mice aged 6–8 weeks by in vivo bioluminescence imaging using an in vivo imaging system (IVIS). An aqueous solution of D-luciferin (150 mg kg$^{-1}$) was injected intraperitoneally 6 h after i.v. injection of 30 µg Luc mRNA-loaded formulations. The pie charts in Figure 2D displayed improved bioluminescence distribution in liver compared with spleen and lung in the groups of ligand-modified LLNs/Luc versus LLNs/Luc without ligands. The bioluminescence distribution and intensity assay (Figures 2D and 2E) clearly showed that the introduction of Chol-PEG$_{400}$-SP, Chol-PEG$_{400}$-Man, and Chol-PEG$_{2000}$-WRK improved Luc mRNA expression in the liver, respectively. Notably, SMW-LLNs/Luc containing three derivatives achieved the highest bioluminescence intensity compared with other groups. Therefore, the formulation of SMW-LLNs was chosen for further optimization.

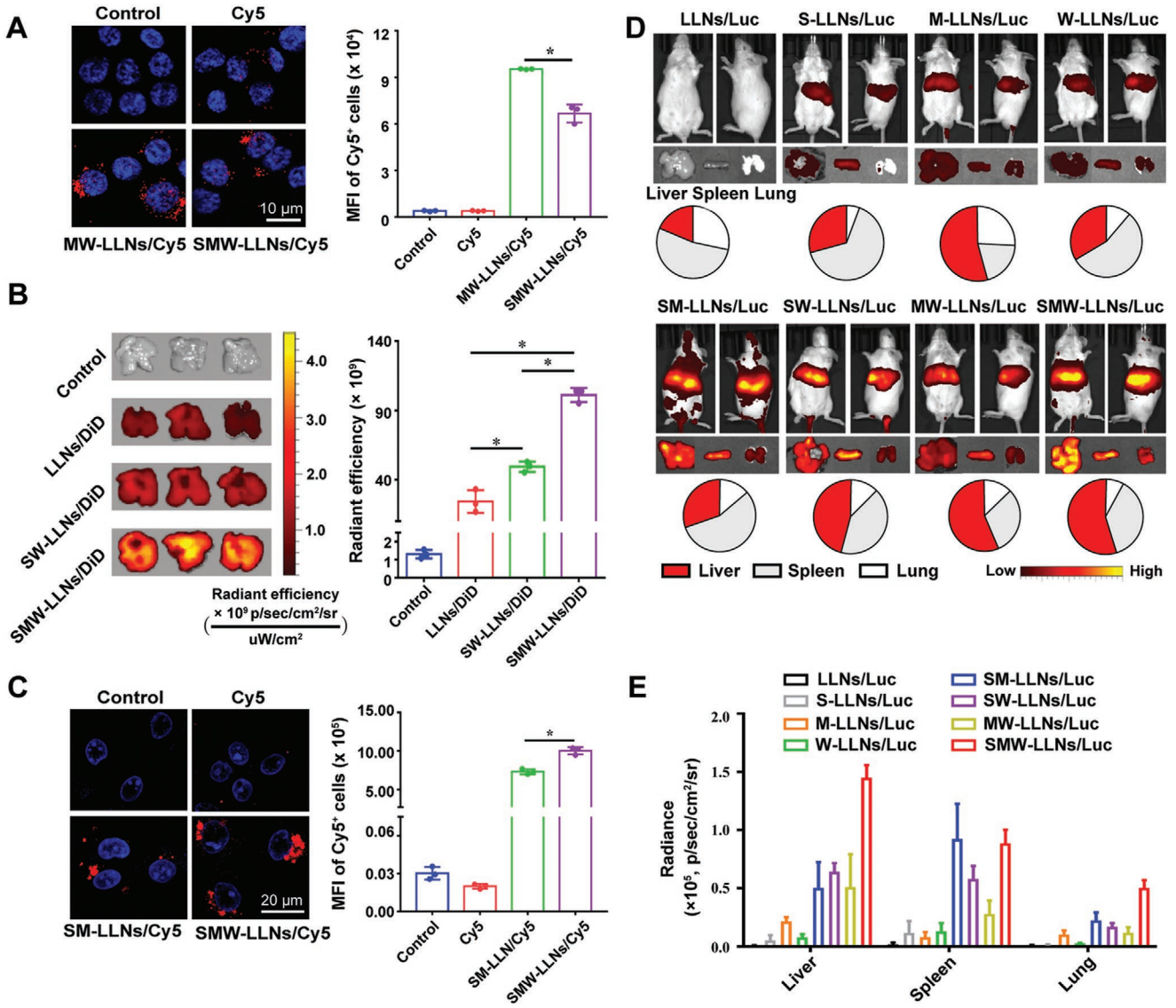


**Figure 2.** Functional verification of Chol-PEG$_{400}$-SP, Chol-PEG$_{400}$-Man, and Chol-PEG$_{2000}$-WRK, respectively. A) CLSM images (left) and FACS analysis (right) of the mean fluorescence intensity of Cy5$^+$ Raw264.7 cells treated by PBS, Cy5, MW-LLNs/Cy5, and SMW-LLNs/Cy5 for 2 h. B) Representative ex vivo images (left) and quantification (right) of liver distribution of DiD-labelled LLNs. C) CLSM images (left) and FACS analysis (right) of the mean fluorescence intensity of Cy5$^+$ LO2 cells treated by PBS, Cy5, SW-LLN/Cy5, and SMW-LLN/Cy5 for 2 h. D) The three cholesterol derivatives can significantly enhance the liver distribution of Luc-mRNA according to the bioluminescence images of mice and major organs when encapsulated into LLNs respectively. Pie charts displayed relative contribution of each organ to total signal. E) Quantification of bioluminescence in major organs after i.v. injection of various LLNs containing 30 μg Luc mRNA.

### 2.2. Optimization of LLNs with CCD Based on the Expression of Luciferase mRNA in Livers

We formulated the three functional cholesterol derivatives into 20 formulations of LLNs according to CCD and mRNA was loaded into the hydrophilic core with a G0-C14-to-mRNA mass ratio of 7.5/1. The formulation before optimization was identified as Origin-LLNs. The particle size of batches of LLNs/mRNA complexes ranged from 125 to 137 nm with a polydispersity index (PDI) < 0.3, while their zeta potential ranged from 33 to 45 mV (Table S1, Supporting Information). The encapsulation efficiency determined by RiboGreen assay was about 70%. There was no significant difference in the size, zeta potential, and encapsulation efficiency among these formulations. Therefore, we concluded that the difference in distribution was mainly caused by the molar ratio of the Chol-PEG$_{400}$-SP, Chol-PEG$_{400}$-Man, and Chol-PEG$_{2000}$-WRK.

Then, CCD was employed to optimize LLNs formulation for liver-targeted mRNA delivery in vivo. Balb/c mice were injected intravenously with the above 20 kinds of LLNs containing 30 μg Luc mRNA with different molar ratios of Chol-PEG$_{400}$-SP ($X_1$), Chol-PEG$_{400}$-Man ($X_2$), and Chol-PEG$_{2000}$-WRK ($X_3$). After treatment for 6 h, the Luc expression ($Y$) of livers was measured by the IVIS (**Figure 3**A). The results from 20 experimental runs

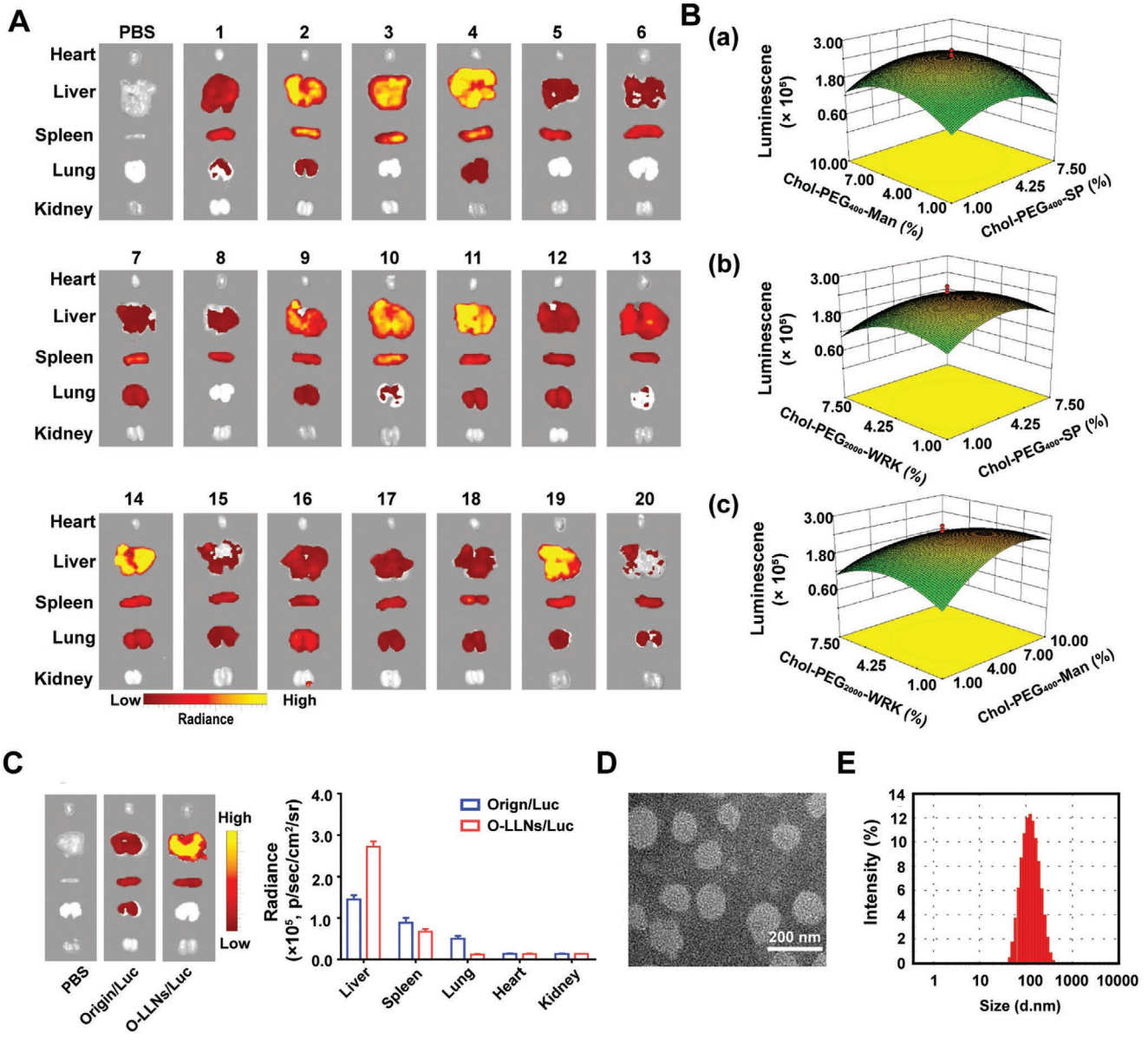


**Figure 3.** Optimization and characterization of mRNA-loaded LLNs. A) Representative distribution of Luc mRNA-loaded LLNs in the CCD. Balb/c mice ($n = 3$) were i.v. injected with LLNs containing 30 μg Luc mRNA and imaged by IVIS after 6 h. B) 3D response surfaces of bioluminescence ($Y$) of liver for the effects of a) Chol-PEG$_{400}$-SP ($X_1$) and Chol-PEG$_{400}$-Man ($X_2$), b) Chol-PEG$_{400}$-SP ($X_1$) and Chol-PEG$_{2000}$-WRK ($X_3$), c) Chol-PEG$_{400}$-Man ($X_2$) and Chol-PEG$_{2000}$-WRK ($X_3$) in the CCD. C) Balb/c mice ($n = 3$) were i.v. injected with Origin-LLNs and O-LLNs carrying 30 μg Luc mRNA, respectively. Ex vivo imaging of organs (left) and quantitative analysis of luminescence (right) were recorded 6 h after injection. D) Representative TEM image of O-LLNs/mRNA. E) The size distribution of O-LLNs/mRNA by DLS.

are shown in Table S1, Supporting Information, and were fitted to a second-order polynomial model, which could be described by the following equation:

$$Y = 2.49 - 1.66X_1 + 0.19X_2 - 0.37X_3 - 0.62X_1^2 - 0.66X_2^2 - 0.54X_3^2 + 0.07X_1X_2 - 0.11X_1X_3 - 0.39X_2X_3 \quad (1)$$

The significance test of regression equation indicated that all three response variables measured in this study showed good fit to the second-order polynomial model (Table S2, Supporting Information). Besides, residual plots by run number and predicted least-squares model were randomly dispersed (Figure S8, Supporting Information), further indicating a good-fitting model. Based on these equations, surface plots of Chol-PEG$_{400}$-SP, Chol-PEG$_{400}$-Man, and Chol-PEG$_{2000}$-WRK as functions of bioluminescence intensity of the liver were presented using Expert Design (Figure 3B). Increasing molar ratio of Chol-PEG$_{400}$-SP, Chol-PEG$_{400}$-Man, and Chol-PEG$_{2000}$-WRK resulted in greater bioluminescence intensity of the liver within a certain range. Accordingly, the optimal ratio of Chol-PEG$_{400}$-SP, Chol-PEG$_{400}$-Man, and Chol-PEG$_{2000}$-WRK in O-LLNs were forecasted to be 4.37%,

6.29%, and 3.38%, respectively. Next, the O-LLNs/Luc mRNA were prepared at the optimal variable settings to evaluate the prediction error of CCD. The bioluminescence intensity of liver treated by the optimized preparation agreed well with that of the theoretical prediction and the bias was less than 5% as shown in Table S3, Supporting Information. Moreover, the bioluminescence intensity in liver using O-LLNs was greater than the Origin-LLNs 6 h after i.v. injection of Luc mRNA (Figure 3C), further suggesting that CCD was a successful optimization process.

The overt Tyndall effect of O-LLNs and O-LLNs/mRNA complex colloidal solution was observed compared with water (Figure S9A,B, Supporting Information). The O-LLN/mRNA complex showed a spherical morphology in the transmission electron microscopy (TEM) image (Figure 3D) and had a mean particle size of 136 nm, measured by dynamic light scattering (DLS) (Figure 3E). The small size allowed O-LLNs/mRNA to pass through the endothelial fenestrae[48] and enter the space of Disse (Figure 1B), thus inducing more interaction with hepatocytes. The surface charge of O-LLNs/mRNA complex was positively charged (zeta potential = 35 mV) (Figure S9C, Supporting Information) and the complete complexation of mRNA was confirmed in agarose gel electrophoresis (Figure S9D, Supporting Information). Moreover, a storage stability assay indicated that mRNA/LLNs could be physically stable at 4 °C for at least 2 weeks (Figure S9E,F, Supporting Information). More systemic investigation is necessary for the long-term storage in the future.

The safety profile of mRNA-loaded O-LLNs was subsequently investigated. The 3-(4,5-dimethylthiazol-2-yl)-2,5-diphenyltetrazolium (MTT) assay was conducted to examine the in vitro toxicity of O-LLNs/mRNA. As shown in Figure S10, Supporting Information, O-LLNs/mRNA with various mRNA concentrations showed negligible cytotoxicity after 24 h (>80% cell viability), indicating an excellent cell compatibility of O-LLNs/mRNA. To study the in vivo toxicity of systemically delivered mRNA by O-LLNs, mice were treated with a single administration of O-LLNs/mRNA, vehicle alone, free mRNA, or phosphate buffer saline (PBS), and key parameters were analyzed 24 h later. No toxicity, as determined by body weight change, was observed for any groups (Figure S11A, Supporting Information). Comparable serum alanine aminotransferase (ALT), aspartate aminotransferase (AST), and total bilirubin (TBIL) levels were found in mice treated with O-LLNs/mRNA nanoparticles, O-LLNs, mRNA, and PBS (Figure S11B–D, Supporting Information). This indicated that there was no significant liver damage caused by the carrier. Next, hematoxylin and eosin (H&E) staining showed no evident lesions in the heart, liver, spleen, lung, and kidney (Figure S11E, Supporting Information). Finally, we evaluated the inflammatory response to PBS, mRNA, O-LLNs, and O-LLNs/mRNA. Serum cytokine (TNF-$\alpha$, IFN-$\gamma$, IL-6, and IL-1$\beta$) levels were measured using an enzyme-linked absorbent assay (ELISA) 24 h after administration. The cytokine concentration was not significantly different among these four groups (Figure S11F–I, Supporting Information). All these results suggested that O-LLNs were one of safer delivery systems.

### 2.3. The Optimized LLNs by CCD Showed Prolonged Systemic Circulation and Facilitated Hepatocyte-Targeted mRNA Delivery In Vivo

The pharmacokinetics and the in vivo uptake of Cy5 mRNA loaded O-LLNs were explored. We injected O-LLNs/Cy5 into healthy C57BL/6 mice via the tail vein. The pharmacokinetic profile was evaluated by calculating the percentage of Cy5 mRNA in blood at various time intervals. O-LLNs/Cy5 significantly extended the circulation of Cy5 mRNA at various time points compared to that of Chol-$PEG_{400}$-SP-free O-LLNs/Cy5 and Origin/Cy5. Moreover, ≈40% of the O-LLNs/Cy5 was still circulating after 30 min, while naked Cy5 mRNA, Origin/Cy5, and O-LLNs/Cy5 (Chol-$PEG_{400}$-SP-free) dropped to 3%, 20%, and 12%, respectively (**Figure 4**A).

To evaluate the uptake of O-LLNs/Cy5 by macrophages in vivo retro-orbital vein blood was collected 4 h after a single administration of O-LLNs/Cy5 to mice. FACS analysis was performed to evaluate uptake of nanoparticle formulations by circulating macrophages. The results showed that O-LLNs/Cy5 significantly inhibited macrophages uptake compared with Chol-$PEG_{400}$-SP-free O-LLNs/Cy5, which was consistent with the in vitro study (Figure 4B). The in vivo uptake of O-LLNs/Cy5 by hepatocytes and non-parenchymal cells was performed after a single i.v. injection. As shown in Figure 4C,D, Cy5 mRNA could be delivered to ≈44% of liver cells. There were 93% hepatocytes ($CD31^-$ $CD45^-$) and 7% immune cells ($CD31^-$ $CD45^+$) among $Cy5^+$ liver cells, while almost no fluorescence was detected in endothelial cells ($CD31^+$ $CD45^-$). These results indicated that O-LLNs were one of potential carriers for in vivo liver-targeted mRNA delivery.

### 2.4. Visualization of Functional Cre mRNA, hEPO mRNA, and mCherry mRNA Delivery Using O-LLNs In Vivo

The ability of O-LLNs to deliver Cre mRNA towards the liver in vivo was studied in Ai9 mice harboring silent tdTomato reporter gene in the ROSA26 gene locus that is conditionally activated in cells expressing Cre protein (**Figure 5**A).[49] To this end, Cre mRNA-loaded O-LLNs (O-LLNs/Cre) were formulated and injected to Ai9 mice via tail veins at the mRNA dosage of 1 mg $kg^{-1}$. The in vivo and ex vivo fluorescence images were measured 3 days post injection, which revealed the expression of Cre mRNA predominantly in liver tissue, second in spleen and lung, the least in heart and kidney, but undetectable in control mice (Figure 5B). For potential use of mRNA therapeutics, it is important to test its functional delivery in various organs and cell subtypes. Thus, the Ai9 mice treated with the O-LLNs/Cre were sacrificed three days later, and the overall 3D distribution of Cre mRNA-targeted cells within organs was visualized using a fluorescence stereoscopic microscopy. As shown in Figure 5C, the livers from Cre mRNA-injected mice but not from control mice showed significant red fluorescence. It can be inferred that O-LLNs/Cre successfully deleted the stop cassette and activated the tdTomato expression in the Ai9 mice livers, demonstrating a functional expression of the transgene tdTomato. Immunohistochemical studies

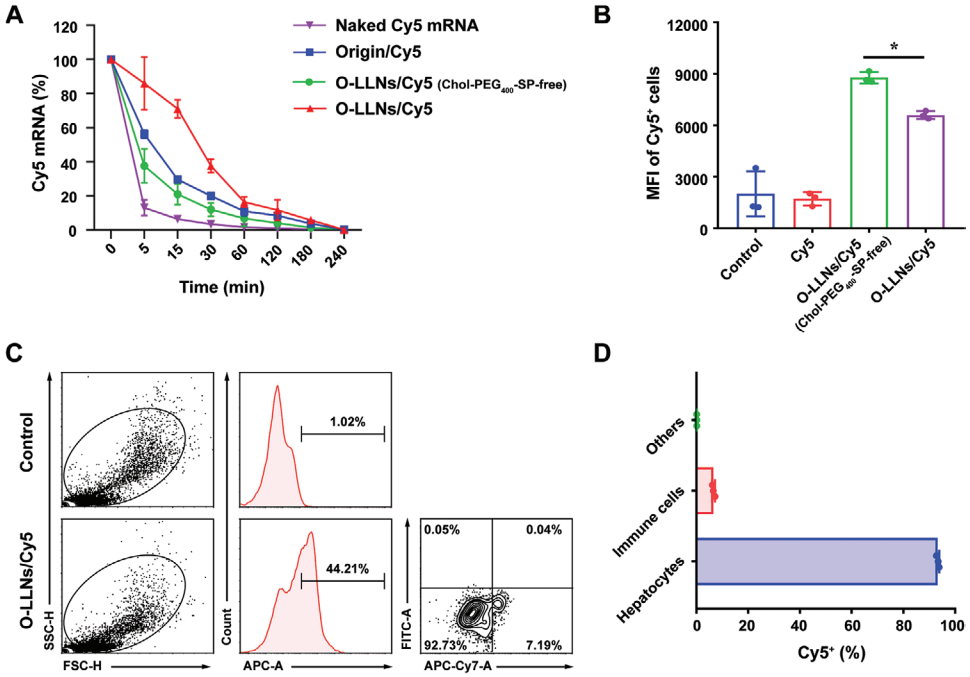


**Figure 4.** The optimized LLNs by CCD showed prolonged systemic circulation and facilitated hepatocyte-targeted mRNA delivery in vivo. A) The circulation profile of O-LLNs/Cy5 in C57BL/6 mice compared to naked Cy5 mRNA, Origin/Cy5, and O-LLNs/Cy5 (Chol-$PEG_{400}$-SP-free). B) The mean fluorescence intensity of $Cy5^+$ macrophages. The retro-orbital vein blood of C57BL/6 mice was analyzed by FACS at 4 h after intravenous administration of PBS, naked Cy5 mRNA, O-LLNs/Cy5 (Chol-$PEG_{400}$-SP-free), and O-LLNs/Cy5, respectively. C,D) The uptake of O-LLNs/Cy5 at the cellular level in livers. C57BL/6 mice were injected with O-LLNs/Cy5. At 4 h after injection, the livers were obtained to quantify the percentage of $Cy5^+$ cells by FACS.

also further confirmed the location and distribution of Cre-activated tdTomato$^+$ (the brown spots) hepatocytes in the liver (Figure 5D). Moreover, the H&E and immunohistochemistry staining revealed that there was no obvious degeneration of hepatocytes, indicating that O-LLNs-mediated liver-specific gene editing might be safe. The western blot assay found dramatically upregulated expression of tdTomato in the livers of Ai9 mice treated by O-LLNs/Cre (Figure 5E), which verified that Cre mRNA was successfully delivered to the liver by O-LLNs and translated into Cre activating tdTomato expression. Additionally, O-LLNs displayed remarkably improved tdTomato expression compared to the LLNs containing DLin-MC3-DMA (MC3), one of the USA approved in vivo nucleic acid delivery systems (Figure 5F).

The mRNA encoding hEPO which is a secretory protein, was subsequently selected to further examine the mRNA delivery ability of O-LLNs. As shown in Figure 5G, O-LLNs/hEPO induced the strongest expression of hEPO in the blood of C57BL/6 mice with intravenous injection of the preparations consisting of hEPO mRNA, compared to Origin/hEPO ($p < 0.001$) and MC3/hEPO ($p < 0.05$). We finally used O-LLNs to deliver the mRNA encoding mCherry to the liver of C57BL/6 mice. It was found that mCherry highly expressed in the albumin antibody-labeled hepatocytes (Figure 5H). Collectively, O-LLNs optimized by CCD were one of highly efficient liver-targeted systems for mRNA delivery according to the investigation of the distribution and functional delivery.

### 2.5. In Vivo Delivery of Cytidine Base Editor mRNA and sgRNA by the O-LLNs in *Pah$^{enu2}$* Mice

Human autosomal recessive liver disease PKU is a type of genetic disease caused by loss-of-function mutations in phenylalanine hydroxylase (PAH) enzyme, which is essential for phenylalanine metabolism.[50] *Pah$^{enu2}$* mice were validated as models for human PKU,[51] which harbored a point mutation in the *Pah* gene on exon 7 (c.835 T>C; p.F263S) that abolished PAH function.[52] We investigated the delivery of mRNA encoding cytosine base editor (CBE) in vivo using O-LLNs to correct the *Pah* gene mutation (**Figure 6**A). The *Pah$^{enu2}$* mice were treated by Origin-LLNs or O-LLNs containing CBE mRNA and sgRNA at a total dose of 1 mg $kg^{-1}$ (mRNA/sgRNA, 1/1, wt/wt). In the end of the experiment, the DNA extracted from the liver biopsies was subjected to PCR amplification and high-throughput sequencing to determine in vivo base editing (C to T mutation) efficiency in liver. Results showed that O-LLNs achieved more than 8% of base editing efficiency, which was 2.36-fold of the Origin-LLNs (Figures 6B and 6C).

As is well-known, the editing efficiency of the editable sites was heterogenous, ranging from less than 5% to nearly 100%. To optimize the editing, we have designed several editing strategies by using spCas9-derived base editors and different sgRNAs. These strategies were tested in a cell model harboring PKU fragment. The approach containing spCas9-derived base editor BE4-Cas9-NG-MAX and sgRNA1-2 was demonstrated to be the most effective one and was used in our in vivo

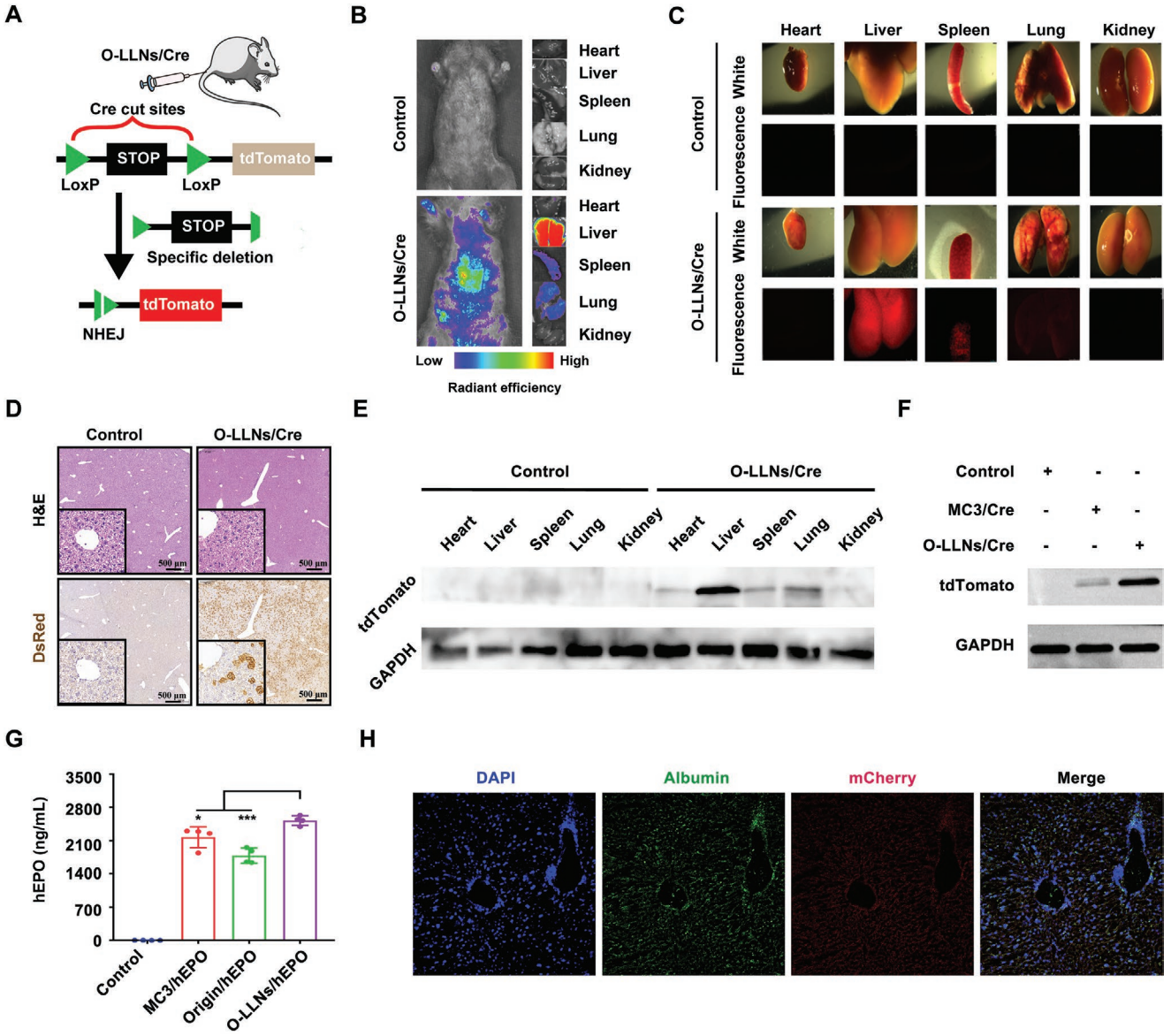


**Figure 5.** O-LLNs optimized by CCD delivered Cre mRNA, hEPO mRNA, and mCherry mRNA with high efficiency in vivo. A) The schematic illustration showed that Cre-loaded nanoparticles deleted the stop cassette and activated tdTomato expression in tdTomato transgenic mice. B) Fluorescence imaging of Ai9 mice injected with O-LLNs/Cre via the tail veins. C) The overall 3D distribution and D) H&E and immunohistochemistry staining of Cre-targeted cells within the liver in normal and Ai9 mice after i.v. injection of O-LLNs/Cre. E) Western blot assay for tdTomato expression in major organs from Ai9 mice at day 3 post injection of O-LLNs/Cre (1 mg $kg^{-1}$). F) Western blot assay for tdTomato expression in the liver from Ai9 mice at day 3 post injection of O-LLNs/Cre or MC3/Cre (1 mg $kg^{-1}$). G) hEPO was quantified using an ELISA assay in serum 24 h post i.v. administration of hEPO mRNA loaded into Origin-LLNs, O-LLNs, or MC3-LLNs (0.75 mg $kg^{-1}$). $^{*}p < 0.05$, $^{***}p < 0.001$. H) Fluorescent images of liver tissues from mice injected with mCherry mRNA-loaded O-LLNs.

experiments. However, even the most effective one generated only 30% editing of the target cytosine (C835T) in vitro (as shown in Figure S12, Supporting Information). The in vivo editing efficiency (8%) we achieved was about 30% of that from the in vitro experiment. So, we're still working on the design and optimization of the high efficiency base editing tools for PKU therapy. Hopefully, these efforts in combination of our rationally designed LLNs will further improve the genome-editing efficiency.

## 3. Conclusion

In summary, we designed a versatile strategy for efficient delivery of mRNA to the liver by utilizing CCD. This tool allowed us to develop an optimized lipid-like nanoparticle with 4.37% Chol-$PEG_{400}$-SP, 6.29% Chol-$PEG_{400}$-Man, and 3.38% Chol-$PEG_{2000}$-WRK, which can synergistically prolong systemic circulation, as well as increase liver targeting and hepatocyte uptake. O-LLNs resulted in functional mRNA delivery to the

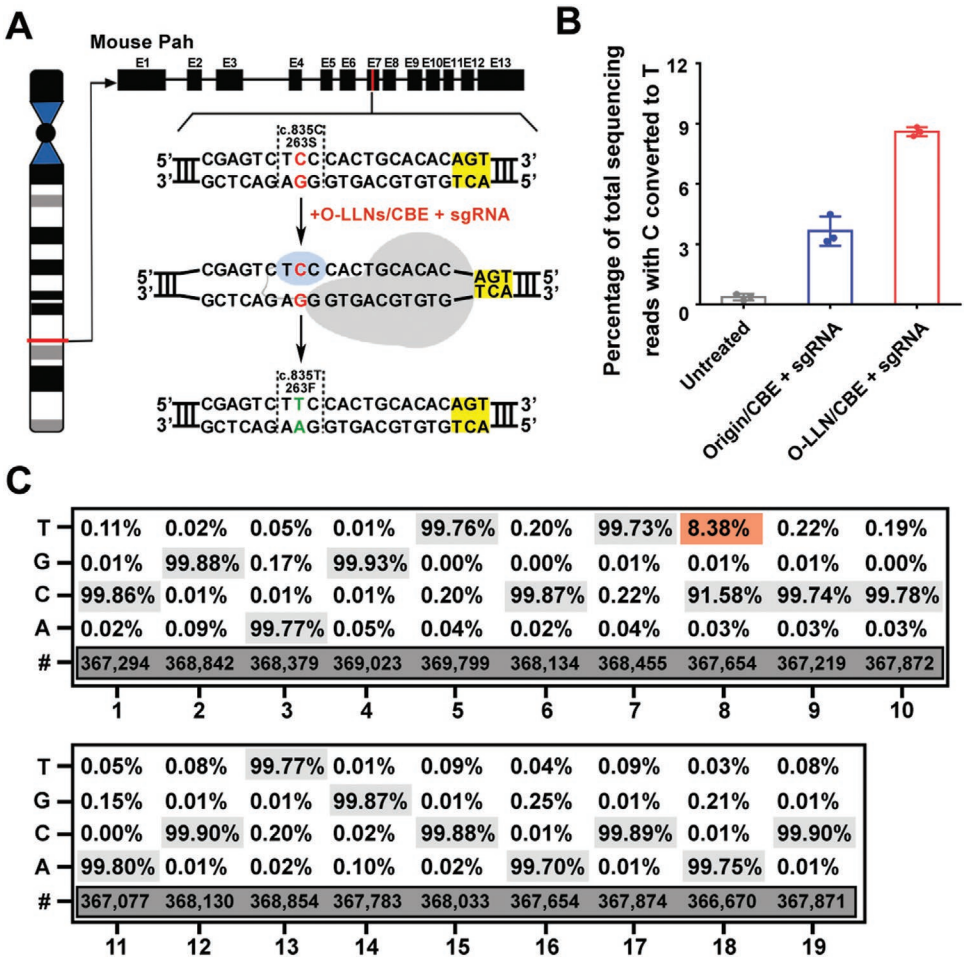


**Figure 6.** In vivo base editing using O-LLNs in *Pah*$^{enu2}$ mice. A) The mutant *Pah*$^{enu2}$ allele harbors the c.835T>C (p.F263S) mutation on Exon 7. The CRISPR-Cas9-associated base editor was designed to correct C>T mutation at position 8 of the sgRNA target. B) In vivo editing efficiencies of the *Pah* gene 7 days after a single i.v. injection of O-LLNs/CBE + sgRNA and Origin/CBE + sgRNA nanoparticles. C) Representative targeted deep sequencing data from mice treated with O-LLNs/CBE + sgRNA.

livers in Ai9 mice and more than 8% base editing efficiency in PKU mice. We envisioned that the use of experimental design in vivo might also be used to optimize nanoparticles for other organs and drug molecules as well. Moreover, it would broaden the therapeutic promise of mRNA delivery and base editing in biomedical fields.

## 4. Experimental Section

*General Procedures*: G0-C14 was synthesized and purified by following published protocols.[32] Cholesterol (Chol) was supplied from Shanghai Yuanju Biology Technology Company (Shanghai, China). DLin-MC3-DMA (MC3), DSPC, and DMG-PEG$_{2000}$ were purchased from Avanti. Firefly luciferase (Luc) mRNA, Cre-recombinase (Cre) mRNA, and human erythropoietin (hEPO) mRNA were obtained from TriLink Biotechnologies (San Diego, CA, United States). Cas9 mRNA and sgRNA were produced using in vitro translation (IVT). D-Luciferin (potassium salt) was purchased from Biovision. Selfpeptide (SP) was purchased from Shanghai Qiangyao Biology Technology Company (Shanghai, China), $W_5R_4K$ (WRK) was purchased from Zhengzhou Paihetaide Pharmaceutical Biotechnology Company (Zhengzhou, China).

*Formulation of mRNA-Loaded LLNs*: The LLNs formulations were formed by a thin-film dispersion method.[53] Briefly, all organic components with specified molar ratios (Table S1, Supporting Information) were dissolved in solvent mixtures of chloroform/ethanol (1:1, v/v) to prepare LLNs. The above solution was removed with a rotary evaporator at 37 °C for 2 h. Then 3 mL RNase-free water was added to rehydrate the lipid film at 60 °C for 30 min to obtain a suspension with a final G0-C14 concentration of 2 mg mL$^{-1}$. Subsequently, the above suspension was sonicated at 85 W for 3 min, then filtered with a 0.22 µm sterilized filter for the following study. mRNA-loaded LLNs formulations were prepared as previously described.[54] Briefly, mRNA was dissolved in RNase-free water, and LLNs and NaCl (1.5 M) were diluted with RNase-free water. The two parts were rapidly mixed to obtain a final weight ratio of 7.5/1 (G0-C14/mRNA) with the final concentration of NaCl of 150 mM, followed by incubation for 10 min at room temperature. For preparation of LLNs/CBE + sgRNA, mRNA and sgRNA (1/1, wt/wt) were dissolved in RNase-free water and mixed, a final weight ratio of G0-C14/(mRNA+sgRNA) was 7.5/1. For preparation of DiD-labelled LLNs, DiD was added in film-forming process to yield a final concentration of 7.5 µg mL$^{-1}$. For preparation of MC3/mRNA, MC3, Chol, DSPC, and DMG-PEG$_{2000}$ (50:38.5:10:1.5 mol ratio) were mixed into a volume of ethanol and three volumes of mRNA (1:16 w/w mRNA to lipid) in citrate buffer were injected into a micro fluidic mixing device

(INano L, Micro&Nano (Shanghai) Biologics Co., Ltd.) at a combined flow rate of 9 mL $min^{-1}$. The resultant mixture was dialyzed in PBS for 24 h to remove ethanol.

*LLNs/mRNA Characterization*: The average particle size, PDI, and zeta potential of LLNs/mRNA formulations were determined by Zetasizer Nano ZS90 (Malvern Instruments, Malvern, United Kingdom). The morphology of the O-LLNs/mRNA was observed by TEM, (H-600, Hitachi, Japan) after proper dilution of O-LLNs/mRNA formulation with 2% phosphotungstic acid solution negative staining. Gel electrophoresis retardation assay was performed to evaluate the complexation of mRNA and LLNs at a G0-C14 to mRNA ratio of 7.5/1 by weight. Free mRNA (0.3 μg) and LLNs/mRNA (containing 0.3 μg mRNA) were diluted with RNase-free water. Subsequently, northernMax formaldehyde loading buffer containing ethidium bromide (50 μg $mL^{-1}$) was added and incubated for 10 min in 65 °C. Following, the samples were electrophoresed in 1% denaturing formaldehyde agarose gel with precooled MOPS buffer at a constant voltage of 180 V for 8 min. The results were analyzed using a ChemiDocTM 219 XRS system (Bio-Rad, United States). The encapsulation efficiency of LLNs/mRNA formulations were determined by RiboGreen assay (Quant-iT RiboGreen RNA assay kit, Invitrogen) according to the manufacturer's instruction.

*mRNA/LLNs Stability*: To study mRNA/LLNs storage stability at 4 °C, the average particle size, PDI, and zeta potential were monitored for 2 weeks.

*Central Composite Design*: A three-factor, five-level CCD was performed to optimize LLNs and determine the optimum levels of these variables. Three independent variables (Chol-$PEG_{400}$-SP mol% ($X_1$), Chol-$PEG_{400}$-Man mol% ($X_2$), and Chol-$PEG_{2000}$-WRK mol% ($X_3$) were studied at five levels coded as $-\alpha$, −1, 0, 1, and $+\alpha$. The value of $\alpha$ is based on $2^{k/4}$ and $k$ represents the number of factors ($\alpha = 1.682$). The variables and their levels for the CCD are shown in Tables S4 and S5, Supporting Information. Three replicates were performed at the center point for a total of 20 experimental runs. Radiance (p $sec^{-1}$ $cm^{-2}$ $sr^{-1}$) of the liver is the dependent variable. The experimental responses of individual influence and the interactions of the three independent variables were studied and modeled through a second-order polynomial equation:

$$Y = b_0 + b_1X_1 + b_2X_2 + b_3X_3 + b_4X_1^2 + b_5X_2^2 + b_6X_3^2 + b_7X_1X_2 + b_8X_1X_3 + b_9X_2X_3 \quad (2)$$

$X_1$, $X_2$, and $X_3$ are the independent variables, and $Y$ is the measured dependent response, $b_0$ the intercept, $b_1$, $b_2$, and $b_3$ the linear coefficients, $b_4$, $b_5$, and $b_6$ the squared coefficients, $b_7$, $b_8$, and $b_9$ the interaction coefficients. In this study, statistical analysis of the data was performed using Expert Design Software version 8.

*Biodistribution Imaging*: For biodistribution studies, mice were intravenously injected with DiD-labeled LLNs at a total dose of 30 μg mRNA. At 2 h after injection, tissues were collected and imaged with an IVIS Lumina system (Perkin Elmer).

*Bioluminescence Imaging*: Distribution of Luc mRNA was evaluated in Balb/c mice aged 6–8 weeks by in vivo bioluminescence imaging using an IVIS Lumina system. An aqueous solution of D-luciferin (150 mg $kg^{-1}$) was injected intraperitoneally 6 h after i.v. injection of 30 μg Luc mRNA-loaded formulations. Bioluminescence signals from live animals or extracted organs (heart, liver, spleen, lung, and kidney) were measured 15 min later with an exposure time of 1 min to ensure that the signal was within effective detection range. Regions of interest were quantified for further analysis.

*In Vitro Toxicity Analysis of O-LLNs/mRNA*: The in vitro toxicity of O-LLNs/mRNA nanoparticles was evaluated using an MTT assay. The cell viability was determined using MTT 24 h post mRNA delivery. LO2 cells were seeded into 96-well plates at $1 \times 10^4$ cells/well and cultured for 24 h. LO2 cells were treated with naked mRNA or O-LLNs/mRNA at various concentrations (0.062, 0.125, 0.250, or 0.500 μg $mL^{-1}$). After incubation for another 20 h, MTT in PBS (5 mg $mL^{-1}$) was added and the cells were incubated for 4 h at 37 °C. The cell culture medium was then carefully removed and 150 μL DMSO was added to each well. The absorbance at 570 nm was measured by a microplate reader (Molecular Devices, USA).

*In Vivo Toxicity Analysis of O-LLNs/mRNA*: All animal experiments were approved by the Animal Experimental Ethics Committee State Key Laboratory of Biotherapy (SKLB) Sichuan University (SCU) (2019.1.1~2020.11.30). C57BL/6 mice aged 6–8 weeks were used to assess the toxicity of intravenously administered formulations (mRNA, O-LLNs, O-LLNs/mRNA, and PBS). After 24 h, whole blood was collected and the serum was isolated at the speed of 5000 rounds per minute (rpm) for 15 min. Biochemical analyses were performed for liver function (ALT, AST, and TBIL) using an automatic analyzer (Hitachi High-Technologies Corp, Minato-ku, Tokyo, Japan). For TNF-$\alpha$, IFN-$\gamma$, IL-6, and IL-1$\beta$ analysis, serum was diluted 1:5. ELISAs were performed using the manufacturer's instruction. In addition, major tissues (heart, liver, spleen, lung, and kidney) were extracted, fixed with 4% formalin solution, embedded in paraffin, sectioned to about 5 μm, and then stained with H&E. Images were acquired on a light microscope (Olympus, Tokyo, Japan). During this time, the body weight of each mouse was monitored.

*In Vitro Cell Uptake*: Confocal imaging and FACS were conducted to study cellular uptake. To verify the inhibiting effect of Chol-$PEG_{400}$-SP on the surface of LLNs on the uptake of phagocytes, Cy5 mRNA-load LLNs (LLNs/Cy5) was prepared as described above. Macrophage-like Raw264.7 cells were seeded at a density of $8 \times 10^4$ cells per well and incubated at 37 °C for 24 h. Then, Raw264.7 cells were treated with 50 μL LLNs/Cy5 (0.5 μg Cy5 mRNA per well) and incubated for 2 h. Next, cells were washed three times with PBS and stained with Hoechst 33258 for 15 min, then imaged by confocal microscopy (LSM 880, Zeiss). Meanwhile, to verify the effect of Chol-$PEG_{2000}$-WRK of LLNs on the uptake of hepatocytes, LO2 cells were treated by the similar methods to Raw264.7 cells. Raw264.7 and LO2 cells were washed three times with PBS and collected. The cells were re-suspended with PBS and analyzed by flow cytometry. All experiments were carried out in triplicate.

To investigate the binding characteristics of Chol-$PEG_{400}$-SP and SIRP$\alpha$ receptor in vitro, Raw264.7 cells were treated with O-LLNs/Cy5 or O-LLNs/Cy5 (Chol-$PEG_{400}$-SP-free) and incubated at 37 °C for 2 h. One group of cells was pre-treated with excess SP for 30 min prior to the addition of O-LLNs/Cy5 or O-LLNs/Cy5 (Chol-$PEG_{400}$-SP-free). The competitive inhibition assay was also conducted using DC2.4 cells overexpressing mannose receptor to explore the binding of Chol-$PEG_{400}$-Man and mannose receptor. DC2.4 cells were treated with O-LLNs/Cy5 or O-LLNs/Cy5 (Chol-$PEG_{400}$-Man-free) and incubated at 37 °C for 2 h. One group of cells was pre-treated with excess mannose for 30 min prior to the addition of O-LLNs/Cy5 or O-LLNs/Cy5 (Chol-$PEG_{400}$-Man-free). Raw264.7 and DC2.4 cells were harvested and washed with PBS. After centrifugation (800 rpm for 3 min), the cells were resuspended in 300 μL PBS and the mean fluorescence of Cy5 was quantified by flow cytometry.

*Pharmacokinetics Study and In Vivo Uptake*: For the in vivo pharmacokinetics study, 8-week-old C57BL/6 mice were divided into four groups ($n = 3$ per group) and intravenously administered with naked Cy5 mRNA, Origin/Cy5, O-LLNs/Cy5 (Chol-$PEG_{400}$-SP-free), and O-LLNs/Cy5 with a dose of 30 μg Cy5 mRNA. Retro-orbital vein blood was obtained using a heparin-coated capillary tube at 0, 5, 15, 30, 60, 120, 180, and 240 min. A microplate reader (Biotek, USA) was used to measure fluorescence intensity of Cy5 at emission and excitation wavelengths of 625 and 670 nm, respectively. Pharmacokinetics was determined by calculating the percentage of Cy5 mRNA in blood at various time intervals, normalized with the initial time point. For the in vivo uptake study of macrophages, retro-orbital vein blood was collected at 4 h. The fluid was incubated with Red Blood Cell Lysis Buffer (BioLegend, USA) to remove red blood cells and centrifuged in 50 mL tubes at 1500 rpm for 5 min. After two washes with PBS, $2 \times 10^6$ cells were treated with purified anti-mouse CD16/32 antibody at 4 °C for 10 min, followed by staining with FITC anti-mouse F4/80 antibody (BioLegend, USA) at 4 °C for 30 min to identify macrophages. Next, cells were washed three times with PBS and suspended in 0.3 mL PBS for FACS analysis. Nanoparticle uptake was quantified on macrophages by Cy5 fluorescence. To test the $Cy5^+$ cells within defined cell type populations of the liver, cell isolation and FACS was performed after 4 h of treatment of O-LLNs/Cy5 (containing 30 μg Cy5 mRNA). Briefly, mice were perfused with

20 mL PBS through the right atrium. Liver was cut and placed in a digestion solution with Collagenase Type II (Biosharp) at 37 °C for 1 h. The cell suspension was passed through a 70 µm mesh and then red blood cells were lysed. Cells were stained to quantify the percentage of $Cy5^+$ cells by FACS. The antibody clones used were: purified anti-mouse CD16/32 Antibody (93, BioLegend), FITC anti-mouse CD31 Antibody (390, BioLegend), and APC/Cyanine7 anti-mouse CD45.2 Antibody (104, BioLegend).

*Gene Editing (O-LLN/Cre mRNA) in the tdTom Mice Model*: O-LLNs/Cre mRNA were prepared as described above and injected into the ROSA26 tdTomato Cre reporter mice (C57BL/6, B6.Cg-Gt (ROSA) 26Sortm9 (CAG–tdTomato) Hze/J), also known as Ai9 mice[55] via tail vein (1mg $kg^{-1}$). Three days later, fluorescence intensity of tdTomato was measured by IVIS and tissues were collected to observe tdTomato expression using fluorescence stereoscopic microscopy (Leica, sGerman).

*Immunohistochemistry*: Immunohistochemical studies were performed using a mouse IHC kit (Beijing Zhongshanjinqiao Biology Technology Company, Beijing, China) on sections of formalin-fixed and paraffin-embedded liver tissues from the above Ai9 mice. Mice treated with PBS were used as control group. Liver sections were deparaffinized with xylene, rehydrated in a graded series of ethanol and water. Endogenous peroxidases were then inactivated in 3% $H_2O_2$ for 30 min, followed by blocking using normal goat serum for 40 min. Then sections were incubated with primary antibodies DsRed Antibody (E-8) (1:1000, Santa Cruz Biotechnology) specific to tdTomato overnight at 4 °C. The sections were washed three times in PBS at room temperature and incubated with biotinylated anti-mouse secondary antibodies at 37 °C for 60 min. Histochemical reactions were carried out using a DAB kit (Beijing Zhongshanjinqiao Biology Technology Company, Beijing, China), and liver sections were counterstained with H&E. Images were generated from a light microscope (Olympus, Tokyo, Japan).

*Western Blot*: O-LLNs/cre-treated, MC3/Cre-treated, and control groups above were transcardially perfused with PBS after euthanasia. The mice organs were removed, cut into pieces, and sonicated in RIPA buffer (New Cell & Molecular Biotech Co., Lid, China) with Protease inhibitor cocktail (Beyotime, China). Later, protein concentrations were analyzed using a BCA kit (Beyotime, China) according to the manufacturer's protocol. The sample was mixed with 5 × SDS-PAGE Sample Loading Buffer (Beyotime, China) and boiled for 5 min. Then 10 µg protein was loaded and separated by 4–20% SDS-PAGE gels (Beijing Zoman Biotechnolgy Co., Lid). The separated proteins were transferred into polyvinylidene fluoride membranes (Millipore, USA), and then blocked for 1 h with 5% skim milk dissolved in 0.1% (w/v) Tween 20 (TBST). The membranes were incubated with primary antibodies overnight at 4 °C (tdTomato (mouse, Santa Cruz, sc-390909), 1:1000 dilution, GAPDH (mouse, Beyotime, AF5009), 1:2000 dilution). After washing three times with PBST, the membranes were incubated with HRP-conjugated anti-Mouse secondary antibodies (Beyotime HRP Goat anti-mouse Ig (H + L), 1:5000 dilution) at RT for 1 h, and then imaged by ChemiScope 6200 Touch system (CliNX, China).

*Immunofluorescence Staining*: C57BL/6 mice received a tail vein injection of mCherry mRNA-loaded O-LLNs carrying 30 µg mCherry mRNA. Mice were sacrificed 6 h post injection, then the livers were harvested and embedded in optimal cutting temperature compound. Tissues were sectioned, stained with albumin Polyclonal antibody Rabbit Polyclonal (Proteintech Group, Inc.) and DAPI, and imaged on a Zeiss LSM 880 confocal microscope.

*In Vivo Therapeutic mRNA Delivery*: C57BL/6 mice were injected intravenously with hEPO mRNA (0.75 mg $kg^{-1}$). At 24 h after i.v. injection, the serum was separated from the whole blood. Subsequently, serum EPO concentrations were detected using Erythropoietin Human ELISA Kit (Jiangsu Jingmei Biotechnolgy Co., Ltd) according to the manufacturer's protocol.

*Base Editing (O-LLNs/CBE + sgRNA) in $Pah^{enu2}$ Mice*: To perform correction of disease-causing mutations in adult tissues in vivo, homozygous $Pah^{enu2}$ mice (6-8 weeks old) were injected with the O-LLNs for co-delivery of CBE mRNA and modified sgRNA at a total dose of 1 mg $kg^{-1}$ (mRNA/sgRNA, 1/1, wt/wt) ($n$ = 3 per group). After 7 days, a liver biopsy was performed for further analyses. Total genome DNA was isolated from the frozen liver tissues using the TIANamp Genomic DNA Kit (TIANGEN, Beijing, China). Genomic regions of interest were amplified by PCR with primers flanked with different barcodes. The products were purified with DNA gel-extraction kit and quantified with NanoDrop (Thermo Fisher). Samples were sequenced commercially using the Illumina Novaseq6000 platform (Tsingke, Beijing and Personal Biotechnology, Shanghai, China).

*Plasmid Transfection*: HEK293T cells were seeded on 96-well plates (BIOFIL). Cells at a confluence of 70–80% were transfected with Transeasy (Forgene) according to the manufacturer's instruction. At 48 h post transfection, 30 µL freshly prepared lysis buffer was added to extract genomic DNA. The mixture was incubated at 55 °C for 10 min and then heat-inactivated at 95 °C for another 10 min. The resulting DNA lysate was subjected to PCR amplification and subsequent analysis.

*Base Editing Analysis with Sanger Sequencing and EditR Software*: Genomic regions of interest were amplified by PCR and analyzed by Sanger sequencing. The sequencing graphs were further quantified by EditR software (baseditr.com) according to the author's description. Primers used for amplifying PKU loci are listed in Table S6, Supporting Information.

*Statistical Analysis*: All values were expressed as mean ± S.D. unless otherwise noted. Data of more than two groups were compared using one-way analysis of variance (ANOVA), and multiple comparisons were performed by Tukey's post-hoc test when determined significantly. Statistical analysis was performed using Graphpad Prism 7.0. P values less than 0.05 were considered statistically significant ($*p < 0.05$, $**p < 0.01$, $***p < 0.001$).

## Supporting Information

Supporting Information is available from the Wiley Online Library or from the author.

## Acknowledgements

Q.Z., F.Q., and R.L. contributed equally to this work. This work was financially supported by the National Natural Science Foundation of China (No. 81872821), National Key S&T Special Projects (2018ZX09201018-024), and Sichuan Province Science and Technology Support Program (20GJHZ0187 and 2019YFH0155).

## Conflict of Interest

The authors declare no conflict of interest.

## Data Availability Statement

Data sharing is not applicable to this article as no new data were created or analyzed in this study.

## Keywords

base editing, central composite design, lipid-like nanoparticles, mRNA delivery

Received: December 23, 2020
Revised: May 11, 2021
Published online:

[1] U. Sahin, K. Karikó, Ö. Türeci, *Nat. Rev. Drug Discovery* **2014**, *13*, 759.
[2] K. A. Hajj, K. A. Whitehead, *Nat. Rev. Mater.* **2017**, *2*, 17056.
[3] W. Y. Zhao, X. C. Hou, O. G. Vick, Y. Z. Dong, *Biomaterials* **2019**, *217*, 119291.
[4] J. B. Miller, S. Y. Zhang, P. Kos, H. Xiong, K. J. Zhou, S. S. Perelman, H. Zhu, D. J. Siegwart, *Angew. Chem., Int. Ed. Engl.* **2017**, *56*, 1059.
[5] Q. Cheng, T. Wei, L. Farbiak, L. T. Johnson, S. A. Dilliard, D. J. Siegwart, *Nat. Nanotechnol.* **2020**, *15*, 313.
[6] J. Liu, J. Chang, Y. Jiang, X. D. Meng, T. M. Sun, L. Q. Mao, Q. B. Xu, M. Wang, *Adv. Mater.* **2019**, *31*, 1902575.
[7] A. C. Komor, Y. B. Kim, M. S. Packer, J. A. Zuris, D. R. Liu, *Nature* **2016**, *533*, 420.
[8] H. A. Rees, D. R. Liu, *Nat. Rev. Genet.* **2018**, *19*, 770.
[9] L. Villiger, H. M. Grisch-Chan, H. Lindsay, F. Ringnalda, C. B. Pogliano, G. Allegri, R. Fingerhut, J. Häberle, J. Matos, M. D. Robinson, B. Thöny, G. Schwank, *Nat. Med.* **2018**, *24*, 1519.
[10] J. M. Levy, W. H. Yeh, N. Pendse, J. R. Davis, E. Hennessey, R. Butcher, L. W. Koblan, J. Comander, Q. Liu, D. R. Liu, *Nat. Biomed. Eng.* **2020**, *4*, 97.
[11] H. Yin, K. J. Kauffman, D. G. Anderson, *Nat. Rev. Drug Discovery* **2017**, *16*, 387.
[12] A. Pickar-Oliver, C. A. Gersbach, *Nat. Rev. Mol. Cell Biol.* **2019**, *20*, 490.
[13] D. Wilbie, J. Walther, E. Mastrobattista, *Acc. Chem. Res.* **2019**, *52*, 1555.
[14] T. T. Jiang, J. M. Henderson, K. Coote, Y. Cheng, H. C. Valley, X. O. Zhang, Q. Wang, L. H. Rhym, Y. Y. Cao, G. A. Newby, *Nat. Commun.* **2020**, *11*, 1979.
[15] C. Q. Song, T. Jiang, M. Richter, L. H. Rhym, L. W. Koblan, M. P. Zafra, E. M. Schatoff, J. L. Doman, Y. Cao, L. E. Dow, L. J. Zhu, D. G. Anderson, D. R. Liu, H. Yin, W. Xue, *Nat. Biomed. Eng.* **2020**, *4*, 125.
[16] X. Zhang, W. Zhao, G. N. Nguyen, C. Zhang, C. Zeng, J. Yan, S. Du, X. Hou, W. Li, J. Jiang, B. Deng, D. W. McComb, R. Dorkin, A. Shah, L. Barrera, F. Gregoire, M. Singh, D. Chen, D. E. Sabatino, Y. Dong, *Sci. Adv.* **2020**, *6*, eabc2315.
[17] K. A. Hajj, J. R. Melamed, N. Chaudhary, N. G. Lamson, R. L. Ball, S. S. Yerneni, K. A. Whitehead, *Nano Lett.* **2020**, *20*, 5167.
[18] B. Li, X. Luo, B. Deng, J. Wang, D. W. McComb, Y. Shi, K. M. Gaensler, X. Tan, A. L. Dunn, B. A. Kerlin, Y. Dong, *Nano Lett.* **2015**, *15*, 8099.
[19] X. Luo, W. Zhao, B. Li, X. Zhang, C. Zhang, A. Bratasz, B. Deng, D. W. McComb, Y. Dong, *Nano Res.* **2018**, *11*, 5596.
[20] Q. Cheng, T. Wei, Y. Jia, L. Farbiak, K. Zhou, S. Zhang, Y. Wei, H. Zhu, D. J. Siegwart, *Adv. Mater.* **2018**, *30*, 1805308.
[21] K. J. Kauffman, J. R. Dorkin, J. H. Yang, M. W. Heartlein, F. DeRosa, F. F. Mir, O. S. Fenton, D. G. Anderson, *Nano Lett.* **2015**, *15*, 7300.
[22] M. A. Oberli, A. M. Reichmuth, J. R. Dorkin, M. J. Mitchell, O. S. Fenton, A. Jaklenec, D. G. Anderson, R. Langer, D. Blankschtein, *Nano Lett.* **2017**, *17*, 1326.
[23] J. C. Kaczmarek, K. J. Kauffman, O. S. Fenton, K. Sadtler, A. K. Patel, M. W. Heartlein, F. DeRosa, D. G. Anderson, *Nano Lett.* **2018**, *18*, 6449.
[24] Y. Li, R. Jarvis, K. Zhu, Z. Glass, R. Ogurlu, P. Gao, P. Li, J. Chen, Y. Yu, Y. Yang, Q. Xu, *Angew. Chem., Int. Ed. Engl.* **2020**, *59*, 14957.
[25] A. Jarzębińska, T, P. , J. Lambrecht, O. Mykhaylyk, L. Kümmerling, P. Beck, G. Hasenpusch, C. Rudolph, C. Plank, C. Dohmen, *Angew. Chem., Int. Ed. Engl.* **2016**, *55*, 9591.
[26] X. Zhao, J. Chen, M. Qiu, Y. Li, Z. Glass, Q. Xu, *Angew. Chem., Int. Ed. Engl.* **2020**, *59*, 20083.
[27] C. D. Sago, M. P. Lokugamage, K. Paunovska, D. A. Vanover, C. M. Monaco, N. N. Shah, M. Gamboa Castro, S. E. Anderson, T. G. Rudoltz, G. N. Lando, P. Munnilal Tiwari, J. L. Kirschman, N. Willett, Y. C. Jang, P. J. Santangelo, A. V. Bryksin, J. E. Dahlman, *Proc. Natl. Acad. Sci. U. S. A.* **2018**, *115*, E9944.
[28] P. P. G. Guimaraes, R. Zhang, R. Spektor, M. Tan, A. Chung, M. M. Billingsley, R. El-Mayta, R. S. Riley, L. Wang, J. M. Wilson, M. J. Mitchell, *J. Controlled Release* **2019**, *316*, 404.
[29] L. Miao, L. Li, Y. Huang, D. Delcassian, J. Chahal, J. Han, Y. Shi, K. Sadtler, W. Gao, J. Lin, J. C. Doloff, R. Langer, D. G. Anderson, *Nat. Biotechnol.* **2019**, *37*, 1174.
[30] T. K. Gündoğdu, İ. Deniz, G. Çalışkan, E. S. Şahin, N. Azbar, *Crit. Rev. Biotechnol.* **2016**, *36*, 368.
[31] H. Yin, R. L. Kanasty, A. A. Eltoukhy, A. J. Vegas, J. R. Dorkin, D. G. Anderson, *Nat. Rev. Genet.* **2014**, *15*, 541.
[32] X. Xu, K. Xie, X. Q. Zhang, E. M. Pridgen, G. Y. Park, D. S. Cui, J. Shi, J. Wu, P. W. Kantoff, S. J. Lippard, R. Langer, G. C. Walker, O. C. Farokhzad, *Proc. Natl. Acad. Sci. U. S. A.* **2013**, *110*, 18638.
[33] R. K. Tsai, D. E. Discher, *J. Cell Biol.* **2008**, *180*, 989.
[34] Q. Chen, C. Wang, X. Zhang, G. Chen, Q. Hu, H. Li, J. Wang, D. Wen, Y. Zhang, Y. Lu, G. Yang, C. Jiang, J. Wang, G. Dotti, Z. Gu, *Nat. Nanotechnol.* **2019**, *14*, 89.
[35] M. Liu, R. S. O'Connor, S. Trefely, K. Graham, N. W. Snyder, G. L. Beatty, *Nat. Immunol.* **2019**, *20*, 265.
[36] S. Subramanian, R. Parthasarathy, S. Sen, E. T. Boder, D. E. Discher, *Blood* **2006**, *107*, 2548.
[37] P. L. Rodriguez, T. Harada, D. A. Christian, D. A. Pantano, R. K. Tsai, D. E. Discher, *Science* **2013**, *339*, 971.
[38] E. Stang, G. M. Kindberg, T. Berg, N. Roos, *Eur. J. Cell Biol.* **1990**, *52*, 67.
[39] A. Brech, S. Magnusson, E. Stang, T. Berg, N. Roos, *Eur. J. Cell Biol.* **1993**, *60*, 154.
[40] S. S. Diebold, C. Plank, M. Cotten, E. Wagner, M. Zenke, *Somatic Cell Mol. Genet.* **2002**, *27*, 65.
[41] G. Ashwell, J. Harford, *Annu. Rev. Biochem.* **1982**, *51*, 531.
[42] M. E. Taylor, J. T. Conary, M. R. Lennartz, P. D. Stahl, K. Drickamer, *J. Biol. Chem.* **1990**, *265*, 12156.
[43] M. E. Taylor, K. Drickamer, *J. Biol. Chem.* **1993**, *268*, 399.
[44] J. Chen, Y. Chen, Y. Cheng, Y. Gao, *Molecules* **2017**, *22*, 1598.
[45] D. Mandal, A. Nasrolahi Shirazi, K. Parang, *Angew. Chem., Int. Ed. Engl.* **2011**, *50*, 9633.
[46] P. G. Dougherty, A. Sahni, D. Pei, *Chem. Rev.* **2019**, *119*, 10241.
[47] H. Tang, L. Yin, K. H. Kim, J. Cheng, *Chem. Sci.* **2013**, *4*, 3839.
[48] H. Sarin, *J. Angiog. Res.* **2010**, *2*, 14.
[49] K. J. Kauffman, M. A. Oberli, J. R. Dorkin, J. E. Hurtado, J. C. Kaczmarek, S. Bhadani, J. Wyckoff, R. Langer, A. Jaklenec, D. G. Anderson, *Mol. Ther.–Nucleic Acids* **2018**, *10*, 55.
[50] N. Blau, F. J. van Spronsen, H. L. Levy, *Lancet* **2010**, *376*, 1417.
[51] A. Shedlovsky, J. D. McDonald, D. Symula, W. F. Dove, *Genetics* **1993**, *134*, 1205.
[52] Z. Ding, P. Georgiev, B. Thöny, *Gene Ther.* **2006**, *13*, 587.
[53] F. Wang, W. Xiao, M. A. Elbahnasawy, X. Bao, Q. Zheng, L. Gong, Y. Zhou, S. Yang, A. Fang, M. M. S. Farag, J. Wu, X. Song, *Front. Pharmacol.* **2018**, *9*, 980.
[54] L. M. Kranz, M. Diken, H. Haas, S. Kreiter, C. Loquai, K. C. Reuter, M. Meng, D. Fritz, F. Vascotto, H. Hefesha, C. Grunwitz, M. Vormehr, Y. Hüsemann, A. Selmi, A. N. Kuhn, J. Buck, E. Derhovanessian, R. Rae, S. Attig, J. Diekmann, R. A. Jabulowsky, S. Heesch, J. Hassel, P. Langguth, S. Grabbe, C. Huber, Ö. Türeci, U. Sahin, *Nature* **2016**, *534*, 396.
[55] T. Wei, Q. Cheng, Y. L. Min, E. N. Olson, D. J. Siegwart, *Nat. Commun.* **2020**, *11*, 3232.